remote sensing

MDPI

Article

Using Satellite Error Modeling to Improve GPM-Level 3 Rainfall Estimates over the Central Amazon Region

Rômulo Oliveira [1,2,*,†], Viviana Maggioni [2], Daniel Vila [1] and Leonardo Porcacchia [2]

[1] Centro de Previsão de Tempo e Estudos Climáticos (CPTEC), Instituto Nacional de Pesquisas Espaciais (INPE), São José dos Campos, SP 12227-010, Brazil; daniel.vila@inpe.br

[2] Sid and Reva Dewberry Department of Civil, Environmental, and Infrastructure Engineering, George Mason University, Fairfax, VA 22030, USA; vmaggion@gmu.edu (V.M.); lporcacc@masonlive.gmu.edu (L.P.)

* Correspondence: romulo.augusto@cptec.inpe.br; Tel.: +55-12-3208-6821

† Current address: Géosciences Environnement Toulouse (GET), Centre National de la Recherche Scientifique, Toulouse 31055, France.

Received: 29 December 2017; Accepted: 21 February 2018; Published: 23 February 2018

Abstract: This study aims to assess the characteristics and uncertainty of Integrated Multisatellite Retrievals for Global Precipitation Measurement (GPM) (IMERG) Level 3 rainfall estimates and to improve those estimates using an error model over the central Amazon region. The S-band Amazon Protection National System (SIPAM) radar is used as reference and the Precipitation Uncertainties for Satellite Hydrology (PUSH) framework is adopted to characterize uncertainties associated with the satellite precipitation product. PUSH is calibrated and validated for the study region and takes into account factors like seasonality and surface type (i.e., land and river). Results demonstrated that the PUSH model is suitable for characterizing errors in the IMERG algorithm when compared with S-band SIPAM radar estimates. PUSH could efficiently predict the satellite rainfall error distribution in terms of spatial and intensity distribution. However, an underestimation (overestimation) of light satellite rain rates was observed during the dry (wet) period, mainly over rivers. Although the estimated error showed a lower standard deviation than the observed error, the correlation between satellite and radar rainfall was high and the systematic error was well captured along the Negro, Solimões, and Amazon rivers, especially during the wet season.

Keywords: global precipitation measurement; IMERG; PUSH; error model; validation; Amazon

1. Introduction

Satellite rainfall estimates have been widely used across Brazil for various purposes, e.g., monitoring natural disasters, hydrological modeling, and climate studies [1–3]. Although the quality of satellite rainfall products has improved significantly in recent decades, such algorithms require careful validation, which provides information about their performance, limitations, and associated uncertainties. Understanding and quantifying errors is also extremely important for algorithm developers to improve the final precipitation products.

Uncertainties in satellite rainfall estimates arise from different factors, including sensor calibration, retrieval errors, and spatial and temporal sampling, among others [4,5]. However, the definition and quantification of uncertainty are directly and indirectly based on the error model definition [6]. Two types of error models are commonly used for assessing uncertainty in precipitation measurements (satellite and radar estimates): additive and multiplicative error models. According to Tian et al. [6], the multiplicative error model is a better choice as it separates the systematic and random errors, can

be applied to a wide range of variability in daily precipitation, and produces superior predictions of the error characteristics.

To understand the nature of the error in satellite precipitation products, a technique to decompose the total error into hit, miss-rain, and false-rain biases [7] is considered. Maggioni et al. [8] proposed the Precipitation Uncertainties for Satellite Hydrology (PUSH) error model framework in order to provide an estimate of the error associated with high-resolution satellite precipitation products for each grid point and at each time step. The probability density function (PDF) of the actual rainfall is modeled differently for missed precipitation cases, false alarms, and hit biases. In the PUSH approach, the error is considered as a combination of random and systematic components and the hit error is modeled with a multiplicative error model [9].

This study aims to assess the characteristics and uncertainty distribution of the Integrated Multisatellite Retrievals for Global Precipitation Measurement (GPM) (IMERG) rainfall estimates over the central Amazon region using the S-band Amazon Protection National System (SIPAM) radar as reference and PUSH as error model. PUSH is calibrated and validated for the study region and takes into account local factors such as seasonality and surface type (i.e., land and river). This work seeks to answer the following scientific questions: (i) What are the characteristics and uncertainty distribution of GPM satellite Level 3 rainfall estimates over the Brazilian Amazon? (ii) How can those uncertainties be minimized to improve satellite precipitation products for use in hydrological applications over the region? In Section 2, the study area, precipitation regime, datasets, and methodology are described. Results of the model calibration and its performance over the study region are presented in Section 3 and discussed in Section 4. Section 5 presents our conclusions and future directions.

2. Study Area, Data, and Methodology

This work focuses on a region located in the middle of the Amazon basin, around the city of Manaus in the state of Amazonas, Brazil. The area covers a radius of 110 km centered at 3.15°S and 59.99°W, where the operational S-band weather radar from the Amazon Protection National System (SIPAM) is located (Figure 1). The characteristics and diurnal cycle of precipitation over the Manaus region have been previously investigated using the S-band SIPAM radar by Oliveira et al. [10], Burleyson et al. [11], Giagrande et al. [12], and Tang et al. [13]. Oliveira et al. [10] suggested that the diurnal cycle of precipitation is strongly modulated by weather systems that produce moderate and heavy rainfall and the rainfall's volume and occurrence, which depend on the season. However, according to Burleyson et al. [11], precipitation varies spatially with a preferred location of maximum rain rate observed east of the Negro River (during the rainy season, from March to May in 2014–2015), driven by the local and large-scale vertical pattern (updrafts and downdrafts) and thermodynamic factors (e.g., diabatic heating) of convective rain cells [12,13].

Oliveira et al. [10] assessed the performance of IMERG in representing the characteristics and diurnal cycle of precipitation over the study region. During the wet (dry) period, the volume and occurrence contributions of moderate (heavy) rainfall are clearly identified and strongly modulated by the precipitation diurnal cycle. A strong dependence of the IMERG dataset performance on seasonality is also observed. This behavior is prominent over the inland water surface type (along the Negro, Solimões, and Amazon rivers) due to the poor calibration of the 2014 Goddard Profiling (GPROF) algorithm (i.e., GMI retrievals) for the continent-ocean surface type.

The precipitation data used for this study are:

i. One National Institute of Meteorology (INMET) rain gauge located in Manaus city (at 3.1°S and 60.0°W). The INMET rain gauge is an automatic station that provides hourly records. This study uses a period of 30 years of daily accumulations (mm·day^{-1});
ii. The S-band SIPAM radar rainfall estimates, processed by Texas A&M University. The rainfall estimates were obtained through the Constant Altitude Plan Position Indicator (CAPPI) product at a 2.5 km vertical level. The radial data were initially gridded to a Cartesian grid with 2 km × 2 km × 0.5 km resolution every 12 min. However, to match the satellite product, the

radar rainfall retrievals were integrated to 30 min and averaged to 0.1 degrees. To reduce the uncertainties of the radar rainfall retrievals, the following criteria were adopted: (i) a radar coverage area of 30–110 km in radius was adopted because of radar physical limitations in detecting signals directly above it ("cone of silence") and far at the constant altitude of 2.5 km; (ii) the areas where the radar beam was blocked by nearby objects were masked out. We refer the reader to Oliveira et al. [10] for a more detailed description of the S-band SIPAM radar and IMERG rainfall retrievals and their performance over the study region;

iii. The Integrated Multisatellite Retrievals for GPM (IMERG)—GPM Level 3 rainfall estimates (V03D, Final run version). The IMERG Final run (research) product is a quasi-global (60° N–S) dataset, with 0.1°/30 min spatial/temporal resolution and currently available for March 2014–present [14,15]. Although newer versions of this product have and will become available, the methodology developed in this work can be easily adapted to any future version of IMERG. By choosing the Final run, which includes a monthly gauge adjustment, we present here the best-case scenario in terms of errors associated with the IMERG product and the worst-case scenario in terms of error correction with PUSH. In other words, the correction scheme would have more room for improvement and look more impressive if applied to the Late or Early near-real-time runs, which lack the bias adjustment.

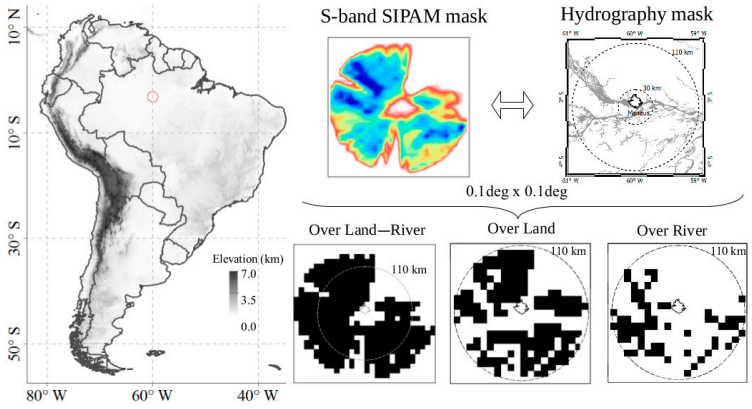

Figure 1. Study area; S-band Amazon Protection National System (SIPAM) radar location in Manaus (in red), Amazonas (AM); and surface class masks (land and river, land only, and river only).

The study period is 12 March 2014 to 17 August 2015 (17 months of half-hourly resolution coincident radar–satellite observations). This period covers the two Intensive Operating Periods (IOPs) of the last Cloud processes of tHe main precipitation systems in Brazil: A contribUtion to cloud resolVing modeling and to the GlobAl Precipitation Measurement (CHUVA) [16] and the Observations and Modeling of the Green Ocean Amazon (GoAmazon) [17] campaigns, held in Manaus city during the wet season, from 1 February to 31 March 2014 (IOP1), and dry season, from 15 August to 15 October 2014 (IOP2). According to Martin et al. [17], the 2014 rainfall regime showed positive precipitation anomalies (~200 mm) during the wet period over the Amazon region. During the dry period, the positive and negative anomalies of rainfall amounts were spatially distributed over the region. In addition, regarding the 2014/15 rainfall regime over the central Amazon region, Marengo et al. [18] found a delay in the 2014/15 onset to January 2015, which resulted in below-normal precipitation. The meteorological context related to the onset/demise of the 2014/5 rainy season over the Manaus region was strongly related to dynamic factors—for example, the Madden–Julian Oscillation (MJO) effect—and was less influenced by thermodynamic factors [18].

Uncertainties associated with the IMERG rainfall estimates over the central Amazon region depend on the surface type and the precipitation regime [10]. Therefore, it is important to investigate and quantify the impact of these factors on the performance of satellite retrievals. The surface type factor consists of a land cover map that discriminates the surface type (in this case, land and inland

water) in the satellite algorithm. Thus, three surface classes (land, river, and land–river) were adopted and investigated separately.

Figure 1 shows the study area, the S-band SIPAM radar 110 km coverage radius, and the masks of the three surface classes, which account for the S-band SIPAM radar limitations. The hydrographic and radar limitation masks are therefore combined and resampled to a $0.1^\circ \times 0.1^\circ$ grid to match the IMERG spatial resolution.

The seasonality factor (precipitation regimes) also plays a fundamental role in the Brazilian Amazon [16–23]. Although the Amazon region presents a very well defined and regionalized dry and wet season pattern [22], such behaviors may vary depending on the year under investigation and the interaction of remote and large-scale phenomena [23]. Liebmann and Marengo [19] developed an objective method of onset and demise identification of the rainy season, later adapted by Liebmann et al. [24], Bombardi and Carvalho et al. [25], and Coelho et al. [26]. The Coelho et al. [26] version is currently operational at the Center for Weather and Climate Studies (CPTEC) (http://clima1.cptec.inpe.br/). The Liebmann and Marengo [19] methodology takes into account the relation between mean precipitation for the pentad ($mm \cdot day^{-1}$) and climatological annual mean daily precipitation ($mm \cdot day^{-1}$) to define the onset and demise of the rainy season.

Thus, IMERG errors are investigated for different surface types (land and inland water) and seasons (dry and wet). The Liebmann and Marengo [19] criterion is used to identify the onset and demise of the rainy and dry seasons in the dataset period. The approach is applied to a single rain gauge station, located within the radar coverage area (Manaus city). Based on the 17 months of IMERG and radar data (coincident time steps), four distinct periods were considered. The time series for calibration and validation (independent period) are defined for both the wet and dry seasons in Table 1. The wet season period used for calibration is consistent with the rainy season characterized by Marengo et al. [18]. The wet season designated for validation includes part of the IOP1. The IOP2 is completely inserted in the calibration dry period. Figure 2 illustrates the precipitation regimes during the wet and dry periods.

Table 1. Precipitation Uncertainties for Satellite Hydrology (PUSH) calibration and validation periods during the wet and dry seasons.

		Periods	Time Steps
Calibration	Dry	15 June 2014–21 December 2014	8043
	Wet	22 December 2014–23 May 2015	6641
Validation	Dry	24 May 2015–17 August 2015	3416
	Wet	12 March 2014–14 June 2014	3865

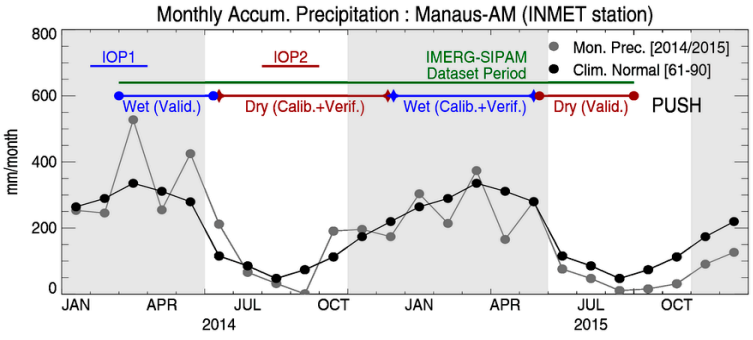

Figure 2. Precipitation regime over Manaus city (National Institute of Meteorology (INMET) station) and wet (blue) and dry (red) periods for PUSH calibration and validation. The shaded area represents the rainy season based on the Climatological Normal (1961–1990) shown with a black line. Wet and dry periods are based on the Liebmann and Marengo [19] criterion, which takes into account the actual observations (gray line). The CHUVA/GoAmazon IOP1 (wet) and IOP2 (dry) periods are also indicated.

The PUSH model, recently developed by Maggioni et al. [8], was adopted to characterize errors associated with IMERG at each grid point and time step. PUSH assesses the probability density function (PDF) of the actual precipitation by decomposing the satellite precipitation error for the following cases: (i) correct no-precipitation detection (Case 00); (ii) missed precipitation events (the satellite records a zero, but the reference detects precipitation, Case 01); (iii) false alarms (the satellite incorrectly detects precipitation, as the reference observes no rain, Case 10); and (iv) hit biases (both satellite and reference detect precipitation, but may disagree on the amount, Case 11).

Given the IMERG satellite observation X and the S-band reference SIPAM radar precipitation observation Y, the PUSH framework provides an estimate of the PDF of the actual precipitation Y at 30 min and 0.1° temporal and spatial resolution. The satellite error can then be computed as either the difference or the ratio between the satellite X and the expected value of the estimated precipitation distribution. PUSH was calibrated for IMERG for different surface types (land and inland water) and seasons (dry and wet) and using a rain/no rain threshold of 0.2 mm·h^{-1}. Once calibration was completed, the model performance was validated during an independent period.

3. Results

3.1. Model Calibration

The PUSH model was calibrated for three separate conditions (over land–river, over river only, and over land only) during the dry and wet seasons over the central Amazon region. The performance of PUSH obtained during the calibration step is briefly described here and presented in the Supplementary Material (Figures S1–S3). The probabilities of correct no-precipitation detection (P00) and missed precipitation (P01 = 1 − P00) for the over land–river, over river only, and over land only surface type conditions were computed for both the dry and wet seasons. Such information provides a general estimate of the probability of false alarms (P10) and hits (P11) for each studied condition (season and surface type).

During the calibration period, IMERG and SIPAM agreed on no rain (RR $\geq$ 0.2 mm·h^{-1}) more than 91% (90%) of the times that the satellite observed no rain during the wet (dry) season over inland water. During both dry and wet seasons, higher (lower) values of P10 (P11) were observed for satellite rainfall greater than 10 mm·h^{-1}, especially over inland water (over river). The exponential curve shows a worse (better) fit over the river (over land), especially during the dry (wet) season, which demonstrates that IMERG poorly reproduces local rain cells along the river. Such behavior indicates the influence of large-scale rainfall events during the wet season, well defined by both precipitation products (Figure S1).

For Case 0 (i.e., when the satellite product records no rain), the model is able to reproduce the reference precipitation distributions both in terms of shape and magnitude for both dry and wet periods and over the three surface types. However, a slight overestimation of the error distribution at low values of satellite precipitation is observed. Similarly, for the cases in which the satellite estimates X are larger than the threshold (i.e., Case 1), the model well reproduced the observed error histograms for all precipitation ranges, in terms of shape and magnitude, during both dry and wet seasons, and for all surface types. Although a slight overestimation (~0.6 mm·h^{-1}) is observed for light precipitation amounts, the estimated distributions are overall very close to the reference histograms during the calibration period (Figures S2 and S3).

3.2. Model Performance

The calibrated model was applied to the independent dry and wet periods in order to validate the model. A first step to evaluate the PUSH performance is to compare the estimated PDF with the reference precipitation distribution for Case 0 and Case 1. Similarly to calibration, during the validation period, the reference PDF shape and magnitude are well reproduced (Figure 3). The differences between estimated and observed PDFs, which are normalized by the reference probability density,

show low positive (negative) values for the first (second) class of observed precipitation (between 0 and 0.2 mm·h^{-1}).

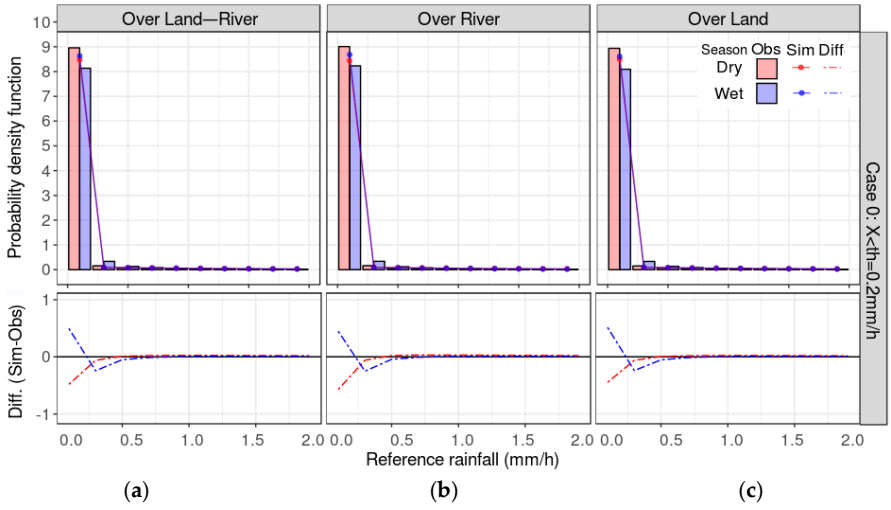

Figure 3. Histogram of the correct no-precipitation detection error (Case 0) for the 0.2 mm h^{-1} threshold over land–river (**a**), river only (**b**), and land only (**c**) during the dry (red) and wet (blue) seasons. Bars indicate the observed probability density function (PDF), dotted lines represent the simulated PDF, and dashed lines are the PDF differences (simulated–observed).

For Case 1, the frequency of several satellite rain rate classes (from 1 to 15 mm·h^{-1}) was compared to the observed precipitation distribution during the validation period (Figure 4). The dry–wet performance difference is evident, especially for light precipitation. In the dry season, negative differences (between 0.4 and 0.6) are observed for satellite precipitation ranging from 1 to 4 mm·h^{-1} and positive differences (~0.5) characterize the over land only surface type. An opposite behavior with a large overestimation of the error distributions is observed during the wet period for all satellite precipitation classes. Moreover, Figure 4 shows poor performance at light rain rates (reference rainfall ~0.5 mm·h^{-1}) over river only, with underestimated (overestimated) probability densities by about 0.6 for almost all the satellite classes during the dry (wet) season.

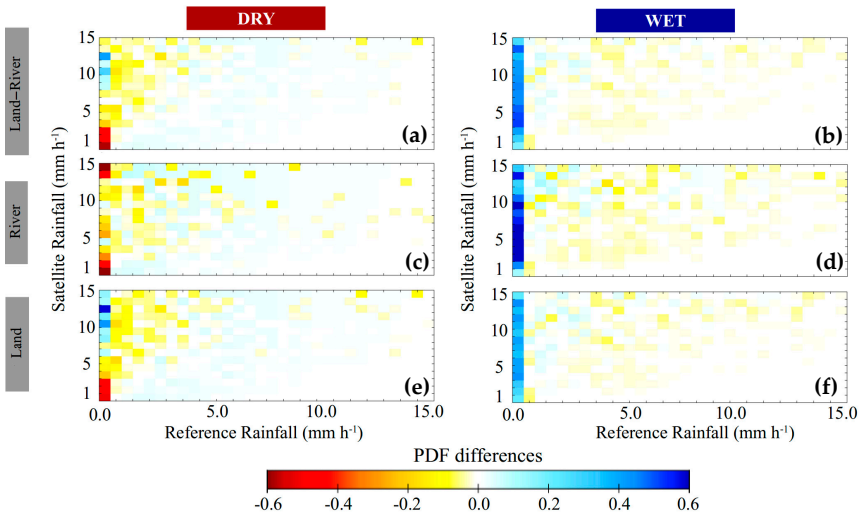

Figure 4. Frequency differences (estimated–observed) (Case 1) for the dry (**left**) and wet (**right**) validation periods and over land–river (**a,b**), river only (**c,d**), and land only (**e,f**), for threshold values of satellite rain rates between 1.0 and 15.0 mm·h^{-1}.

The error spatial distributions were then investigated in order to better understand the model performance over different surface types during one precipitation event in the dry season (06:30–06:59 UTC on 28 May 2015) and one during the wet season (04:00–04:29 UTC on 12 March 2014). Figures 5 and 6 show (i) the observed error (left panels), computed as the difference between IMERG and S-band SIPAM radar; the estimated error (middle panels), computed as the difference between the S-band SIPAM radar and the mean of the modeled distribution; and (ii) the scatterplots of estimated versus observed errors (right panels), together with the corresponding correlation coefficients.

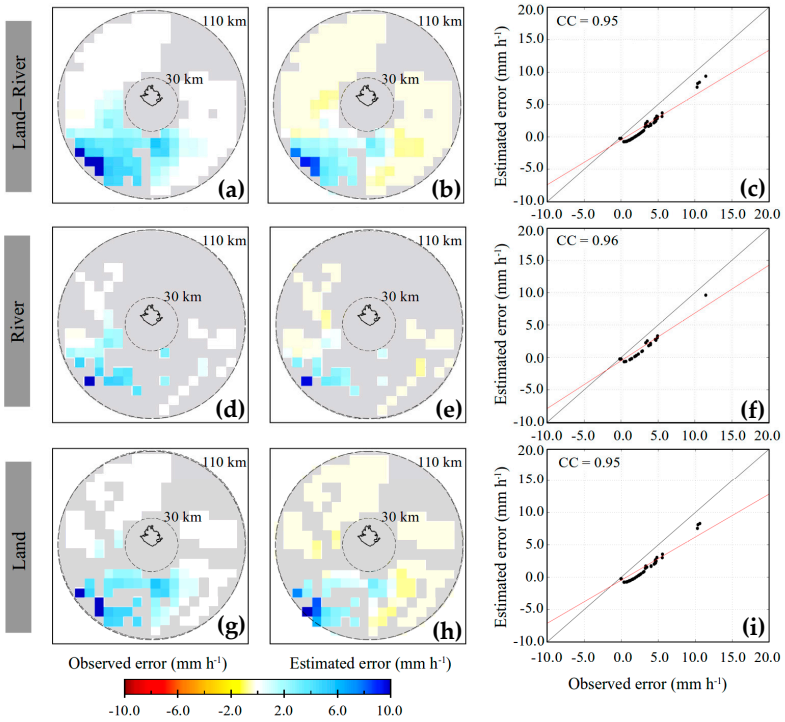

Figure 5. Comparisons of observed and estimated errors during a single time step (06:30–06:59 UTC on 28 May 2015) over land–river (**a**–**c**), river only (**d**–**f**), and land only (**g**–**i**), during the dry validation period. The observed error is defined as the difference between the Integrated Multisatellite Retrievals for Global Precipitation Measurement (IMERG) satellite retrieval and the S-band SIPAM radar observation. The estimated error is defined as difference between the satellite and the estimated reference precipitation (not shown). The scatterplots (**c**,**f**,**i**) show estimated error versus observed error.

PUSH adequately reproduced the spatial intensity patterns of the error in both precipitation events. Nevertheless, the error model clearly underestimates (~−0.5 mm·h^{-1}) light precipitation for both the dry and wet seasons. The estimated error did not reproduce correctly the satellite underestimations, presenting less underestimation than the observed error. On the other hand, the model shows good performance at large rain rates, when the satellite greatly overestimates precipitation. The scatterplots confirm the agreement between observed and estimated errors, with some overestimation of the error at low satellite rain rates. The correlation coefficient presented values between 0.93 and 0.96, slightly varying depending on the surface type conditions and season. However, no remarkable difference in the model performance was observed for different conditions, which shows independent calibration of the error model for different surface types and seasons.

To further evaluate the PUSH performance, Figure 7 demonstrates its long-term ability to reproduce the error in terms of intensity and spatial distribution. The standard deviation (SD) of both the observed and estimated errors and their correlation coefficient (COR) were computed for the validation dry and wet periods. In order to investigate the influence of the surface type on the error spatial distribution, the over land and over river observed and estimated errors were combined and

analyzed. It is evident for both periods that the modeled error produced lower SD values than did the observed differences, indicating less error variability. However, the spatial distribution patterns of the errors look similar to each other, regardless of the period. The wet period is also characterized by a higher SD than is the dry one, when IMERG largely overestimates the precipitation observed by the S-band SIPAM radar, especially along the river. The maximum SD values for the observed and modeled errors are about 2.2 mm·h^{-1} and 2.0 mm·h^{-1} for the dry season and 3.0 mm·h^{-1} and 2.5 mm·h^{-1} for the wet season, respectively. The spatial distributions of the temporal COR show most values between 0.8 and 1 during both dry and wet periods. However, the highest COR values were concentrated along the river and during the wet season.

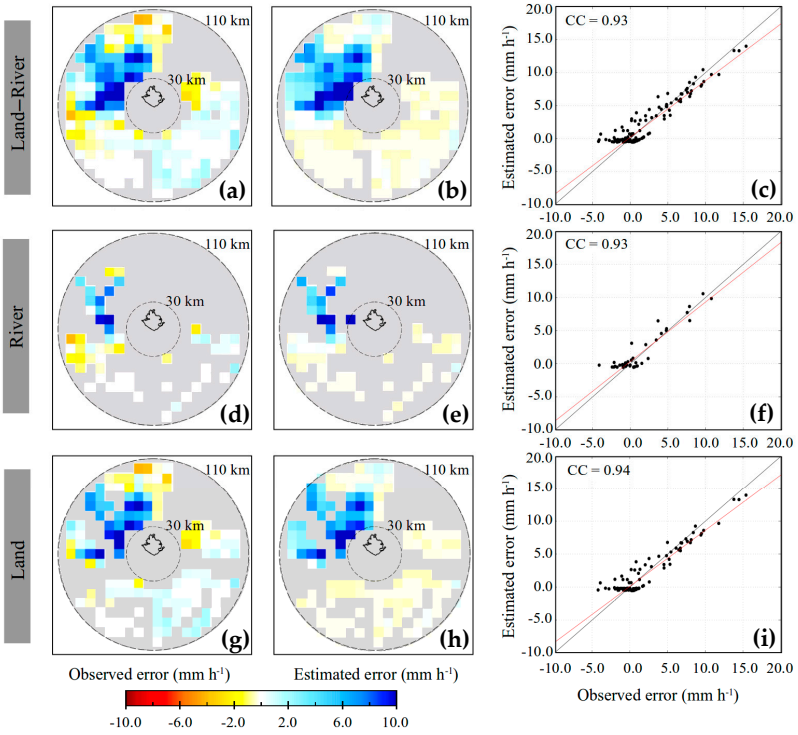

Figure 6. As in Figure 5, but for the wet validation period (04:00–04:29 UTC on 12 March 2014).

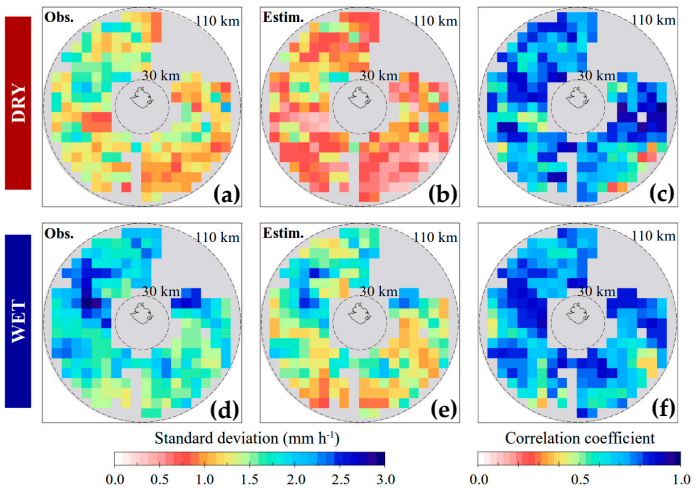

Figure 7. Spatial distributions of the standard deviation of (**a**,**d**) observed and (**b**,**e**) estimated errors and their (**c**,**f**) correlation coefficients over the dry (upper) and wet (lower) seasons.

3.3. Satellite Precipitation Product Correction

The original IMERG product was then corrected using the PUSH modeled errors, according to the following relationship:

$$Xc = X + E \quad (1)$$

where Xc is the "corrected" IMERG rainfall estimates, X is the original IMERG rainfall estimates, and E is the estimated error obtained via PUSH. The performance of the corrected IMERG was evaluated for different surface types and seasons and compared with the original IMERG. Both continuous and categorical scores were used as performance metrics and are shown in Figure 8 in the form of (i) a Taylor diagram [27], which summarizes how closely a dataset matches a reference using COR, root mean square error (RMSE), and SD; and (ii) a Performance diagram [28], which utilizes the geometric relationship between success ratio (SR), which is represented by 1 − False Alarm Ratio (FAR), the probability of detection (POD), bias score (BIAS), and the critical success index (CSI) to display all four metrics simultaneously. A seasonal dependence, which is strongly linked to the precipitation regime in the region, is observed in both the Taylor and Performance diagrams and corroborates the results in Oliveira et al. [10]. The dry period presents a clear underperformance in comparison with the wetter period, especially in the categorical metrics (Figure 8b).

The corrected IMERG presents a slightly better performance than does the original IMERG, particularly in the continuous scores shown in the Taylor diagram. The COR for all the conditions increased from ~0.1 to 0.2 during the dry period and from ~0.3 to 0.4 during the wet period. The most notable improvement is observed in the normalized SD and RMSE scores. This indicates that the corrected IMERG estimates are closer to the S-band radar rainfall estimates (reference) than are those of the original IMERG product.

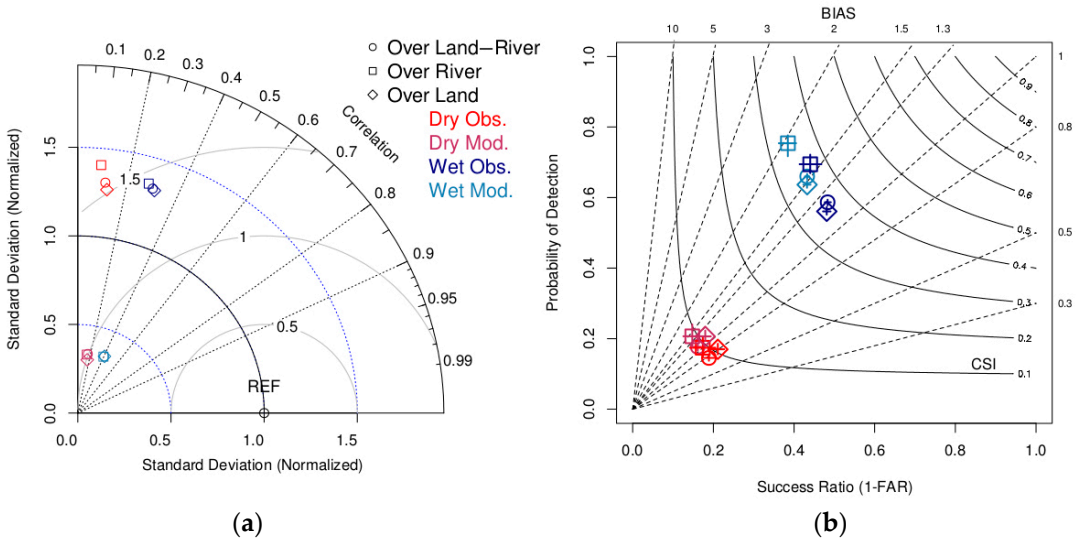

Figure 8. Taylor diagram (**a**) and performance diagram (**b**) showing dry and wet metrics of the IMERG original rainfall estimates versus IMERG modeled via the PUSH model, for different surface types over the Manaus region and for the validation period. In (**a**), the angular axes show COR; whereas radial axes (blue lines) show the SD, normalized against the reference; and the centered RMS difference is represented by the solid gray line. In (**b**), dashed lines represent bias scores with labels on the outward extension of the line; the labeled solid contours correspond to CSI; the x- and y-axis represent the SR and POD, respectively; and sampling uncertainty is given by the crosshairs.

4. Discussion

The novelty of this study consists in investigating the error characteristics of the recently developed IMERG rainfall products over a tropical area characterized by distinct surface type classes

(e.g., forest, nonforest, hydrology, and urban areas), i.e., the central Amazon region. Specifically, this work proposes a novel framework to correct these estimates that have the potential to be used in hydrological predictions and water resource management across the globe. In order to expand our results to other regions, a seasonal surface-type-based analysis was performed.

During the calibration period, PUSH presented promising results for estimating the error associated with satellite rainfall products at moderate to heavy rainfall rates, as shown by results in Section 3.1. The validation results presented in Section 3.2 suggest that the PUSH error model could efficiently characterize the IMERG error along the Negro, Solimões, and Amazon rivers, especially during the wet season. Furthermore, results presented in Section 3.3 showed that the PUSH-corrected IMERG exhibited improvements in the continuous statistics with respect to the original IMERG dataset. However, no significant improvements were observed in the categorical statistics, which suggests that the ability to detect local characteristics, especially during the dry season (i.e., local convection) depends more on the physical assumptions within the satellite rainfall retrieval algorithms. One option would be, for instance, to exploit other passive microwave channels to minimize the uncertainty related to the bright band for surface rainfall retrievals, among others.

Such findings are of fundamental importance to the correct and successful application of GPM-based rainfall estimates in several applications, like natural disaster monitoring, data assimilation systems, hydrological modeling, climatic studies, and for better understanding of the physical processes of precipitation systems over the Amazon region. Moreover, our results provide useful information for satellite precipitation algorithm developers and contribute to meliorating the GPM products.

5. Conclusions

In this study, the characteristics of errors associated with the GPM IMERG final product were investigated over the central Amazon region using an S-band radar as reference. The analysis was performed comparing the dry and wet seasons during March 2014 and August 2015. The PUSH error framework, originally proposed by Maggioni et al. [8], was calibrated and validated for the study region, and expanded to take into account local factors like seasonality and surface types (i.e., land and river).

Results showed that the PUSH model was able to reproduce the error between the IMERG product and the S-band SIPAM radar ground observations. During the calibration period, PUSH could capture the overall spatial pattern of precipitation for both seasons and surface types. However, the model exhibited limited capability in characterizing light precipitation and associated errors. For Case 0 (i.e., when the satellite product detects no rain), PUSH slightly overestimated the rainfall during both dry and wet seasons. A slight (but not significant) overestimation of light rain rates was also observed for Case 1 (i.e., when the satellite product detects rain) for all conditions. During the validation period, PUSH was able to efficiently predict the error distributions during dry and wet periods. However, an underestimation (overestimation) of light rain rates was observed during the dry (wet) period. Such behavior was clearly detected in Case 0 (for rain rate classes lower than 0.2 $mm \cdot h^{-1}$) and for Case 1, especially over the river.

Overall, the PUSH-modeled error presented similar spatial and intensity distributions when compared with the observed error. Although the estimated errors have a lower standard deviation than the observed error, there is a high correlation between the two and a good capability in capturing the error along the Negro, Solimões, and Amazon rivers, especially during the wet season. Lastly, the PUSH-corrected IMERG product presented a slight improvement with respect to the original IMERG dataset during the validation period. The improvement was more evident in the continuous statistical metrics than in the categorical ones. Future studies should focus on investigating and separating the random and systematic error components and on verifying the viability of using PUSH to correct IMERG products in other regions of Brazil and beyond.

Supplementary Materials: The following are available online at www.mdpi.com/2072-4292/10/2/336/s1. Figure S1. Probability of false alarm (P10) (upper panels) and probability of hit (P11) (lower panels) for a minimum threshold of 0.2 mm·h^{-1} over land–river (green), over river only (red), and over land only (blue), during the dry (left panels) and wet (right panels) seasons. Figure S2. Distributions of correct no-precipitation detection errors (Case 0) for the 0.2 mm·h^{-1} threshold over land–river (a), over river only (b), and over land only (c), during the dry (red) and wet (blue) seasons (calibration period). Bars indicate the observed PDF, dotted lines represent the simulated PDF, and dashed lines show the PDF differences (simulated–observed). Figure S3. PDF from observations (bars) and simulated by the error model (black lines) and their differences (estimated minus observed probability densities) for the dry (in red) and wet (in blue) calibration periods and over land–river (a,d), over river only (b,e), and over land only (c,f). Examples for threshold values of satellite rain rates of 2.5 and 10.0 mm·h^{-1}.

Acknowledgments: The first author acknowledges financial support from the National Council for Scientific and Technological Development (CNPq) and the Coordination for the Improvement of Higher Education Personnel (CAPES) Brazil during his PhD. studies and also the Institutional Program of Overseas Sandwich Doctorate (PDSE) from CAPES (process 6836-15-1) for the internship opportunity. The authors also acknowledge the CHUVA Project (FAPESP Grant 2009/15235-8), the Amazon Protection National System (SIPAM), Texas A&M University (TAMU), and NASA/Goddard Space Flight Centers and Precipitation Processing System (PPS) for the data provided for this study, and Aaron Funk and Mári Firpo for the data and methodology support. The IMERG datasets are provided by NASA/PPS and are available at https://pmm.nasa.gov/data-access/downloads/gpm. The ground radar data from SIPAM/TAMU are available at http://chuvaproject.cptec.inpe.br.

Author Contributions: Rômulo Oliveira designed the study, conducted the analysis and wrote the manuscript. Viviana Maggioni, Daniel Vila, and Leonardo Porcacchia contributed to discussions and revisions, providing important feedback and suggestions.

Conflicts of Interest: The authors declare no conflict of interest.

References

1. Espinoza, C.; Marengo, J.A.; Ronchail, J.; Carpio, J.M.; Flores, L.N.; Guyot, J.L. The extreme 2014 flood in south-western Amazon basin, the role of tropical-subtropical South Atlantic SST gradient. *Environ. Res. Lett.* **2014**, *9*, 124007. [CrossRef]
2. Falck, A.S.; Maggioni, V.; Tomasella, J.; Vila, D.A.; Diniz, F.L.R. Propagation of satellite precipitation uncertainties through a distributed hydrologic model: A case study in the Tocantins-Araguaia basin in Brazil. *J. Hydrol.* **2014**, *527*, 943–957. [CrossRef]
3. de Oliveira, N.S.; Rotunno Filho, O.C.; Marton, E.; Silva, C. Correlation between rainfall and landslides in Nova Friburgo, Rio de Janeiro-Brazil: A case study. *Environ. Earth Sci.* **2016**, *75*, 1358. [CrossRef]
4. Hong, Y.; Hsu, K.-L.; Moradkhani, H.; Sorooshian, S. Uncertainty quantification of satellite precipitation estimation and monte carlo assessment of the error propagation into hydrologic response. *Water Resour. Res.* **2006**, *42*, 1–15. [CrossRef]
5. Tang, L.; Tian, Y.; Yan, F.; Habib, E. An improved procedure for the validation of satellite-based precipitation estimates. *Atmos. Res.* **2015**, *163*, 61–73. [CrossRef]
6. Tian, Y.; Huffman, G.J.; Adler, R.F.; Tang, L.; Sapiano, M.; Maggioni, V.; Wu, H. Modeling errors in daily precipitation measurements: Additive or multiplicative? *Geophys. Res. Lett.* **2013**, *40*, 2060–2065. [CrossRef]
7. Tian, Y.; Peters-Lidard, C.; Eylander, J.; Joyce, R.; Huffman, G.; Adler, R.; Hsu, K.; Turk, F.; Garcia, M. Component analysis of errors in satellite-based precipitation estimates. *J. Geophys. Res.* **2009**, *114*, D24101. [CrossRef]
8. Maggioni, V.; Sapiano, M.; Adler, R.; Tian, Y.; Huffman, G. An error model for uncertainty quantification in high-time-resolution precipitation products. *J. Hydrometeorol.* **2014**, *15*, 1274–1292. [CrossRef]
9. Maggioni, V.; Sapiano, M.R.P.; Adler, R.F. Estimating uncertainties in high-resolution satellite precipitation products: Systematic or random error? *J. Hydrometeorol.* **2016**, *17*, 1119–1129. [CrossRef]
10. Oliveira, R.; Maggioni, V.; Vila, D.; Morales, C. Characteristics and diurnal cycle of GPM rainfall estimates over the central Amazon region. *Remote Sens.* **2016**, *8*, 544. [CrossRef]
11. Burleyson, C.; Feng, Z.; Hagos, S.; Fast, J.; Machado, L.; Martin, S. Spatial Variability of the Background Diurnal Cycle of Deep Convection around the GoAmazon2014/5 Field Campaign Sites. *J. Appl. Meteorol. Climatol.* **2016**. [CrossRef]
12. Giangrande, S.E.; Toto, T.; Jensen, M.P.; Bartholomew, M.J.; Feng, Z.; Protat, A.; Williams, C.R.; Schumacher, C.; Machado, L. Convective cloud vertical velocity and mass-flux characteristics from radar wind profiler observations during GoAmazon2014/5. *J. Geophys. Res. Atmos.* **2016**, *121*, 891–913. [CrossRef]

13. Tang, S.; Xie, S.; Zhang, Y.; Zhang, M.; Schumacher, C.; Upton, H.; Jensen, M.P.; Johnson, K.L.; Wang, M.; Ahlgrimm, M.; et al. Large-scale vertical velocity, diabatic heating and drying profiles associated with seasonal and diurnal variations of convective systems observed in the GoAmazon2014/5 experiment. *Atmos. Chem. Phys.* **2016**, *16*, 14249–14264. [CrossRef]
14. Huffman, G.J.; Bolvin, D.T.; Braithwaite, D.; Hsu, K.; Joyce, R.; Xie, P. *GPM Integrated Multi-Satellite Retrievals for GPM (IMERG) Algorithm Theoretical Basis Document (ATBD)*; National Aeronautics and Space Administration (NASA): Washington, DC, USA, 2015. Available online: http://pmm.nasa.gov/sites/default/files/document_files/IMERG_ATBD_V4.4.pdf (accessed on 10 August 2016).
15. Huffman, G.J.; Bolvin, D.T.; Nelkin, E.J. *Integrated Multi-Satellite Retrievals for GPM (IMERG) Technical Documentation*; National Aeronautics and Space Administration (NASA): Washington, DC, USA, 2015. Available online: http://pmm.nasa.gov/sites/default/files/document_files/IMERG_doc.pdf (accessed on 10 August 2016).
16. Machado, L.A.T.; Silva Dias, M.A.F.; Morales, C.; Fisch, G.; Vila, D.; Albrecht, R.; Goodman, S.J.; Calheiros, A.J.P.; Biscaro, T.; Kummerow, C.; et al. The CHUVA Project. How Does Convection Vary across Brazil? *Bull. Am. Meteorol. Soc.* **2014**, *95*, 1365–1380. [CrossRef]
17. Martin, S.T.; Artaxo, P.; Machado, L.A.T.; Manzi, A.O.; Souza, R.A.F.; Schumacher, C.; Wang, J.; Andreae, M.O.; Barbosa, H.M.J.; Fan, J.; et al. Introduction: Observations and Modeling of the Green Ocean Amazon (GoAmazon2014/5). *Atmos. Chem. Phys.* **2016**, *16*, 4785–4797. [CrossRef]
18. Marengo, J.A.; Fisch, G.F.; Alves, L.M.; Sousa, N.V.; Fu, R.; Zhuang, Y. Meteorological context of the onset and end of the rainy season in Central Amazonia during the GoAmazon2014/5. *Atmos. Chem. Phys.* **2017**, *17*, 7671–7681. [CrossRef]
19. Liebmann, B.; Marengo, J. Interannual variability of the rainy season and rainfall in the Brazilian Amazon Basin. *J. Clim.* **2001**, *14*, 4308–4318. [CrossRef]
20. Machado, L.; Laurent, H.; Dessay, N.; Miranda, I. Seasonal and diurnal variability of convection over the Amazonia: A comparison of different vegetation types and large scale forcing. *Theor. Appl. Climatol.* **2004**, *78*, 61–77. [CrossRef]
21. Satyamurty, P.; De Castro, A.A.; Tota, J.; Gularte, L.E.S.; Manzi, A.O. Rainfall trends in the Brazilian Amazon basin in the past eight decades. *Theor. Appl. Climatol.* **2010**, *99*, 139–148. [CrossRef]
22. Santos, E.B.; Lucio, P.S.; Silva, C.M.S. Precipitation regionalization of the Brazilian Amazon. *Atmos. Sci. Lett.* **2015**, *16*, 185–192. [CrossRef]
23. Villar, J.C.E.; Ronchail, J.; Guyot, J.L.; Cochonneau, G.; Naziano, F.; Lavado, W.; Oliveira, E.D.; Pombosa, R.; Vauchel, P. Spatio-temporal rainfall variability in the Amazon basin countries (Brazil, Peru, Bolivia, Colombia, and Ecuador). *Int. J. Climatol.* **2009**, *29*, 1574–1594. [CrossRef]
24. Liebmann, B.; Camargo, S.J.; Seth, A.; Marengo, J.A.; Carvalho, L.M.; Allured, D.; Fu, R.; Vera, C.S. Onset and End of the Rainy Season in South America in Observations and the ECHAM 4.5 Atmospheric General Circulation Model. *J. Clim.* **2007**, *20*, 2037–2050. [CrossRef]
25. Bombardi, R.J.; Carvalho, L.M.V. IPCC global coupled model simulations of the South America monsoon system. *Clim. Dyn.* **2009**, *33*, 893–916. [CrossRef]
26. Coelho, C.A.S.; Cardoso, D.H.F.; Firpo, M.A.F. Precipitation diagnostics of an exceptionally dry event in Sao Paulo, Brazil. *Theor. Appl. Climatol.* **2016**, *125*, 769–784. [CrossRef]
27. Taylor, K.E. Summarizing multiple aspects of model performance in a single diagram. *J. Geophys. Res.* **2001**, *106*, 7183–7192. [CrossRef]
28. Roebber, P.J. Visualizing multiple measures of forecast quality. *Weather Forecast.* **2009**, *24*, 601–608. [CrossRef]

© 2018 by the authors. Licensee MDPI, Basel, Switzerland. This article is an open access article distributed under the terms and conditions of the Creative Commons Attribution (CC BY) license (http://creativecommons.org/licenses/by/4.0/).